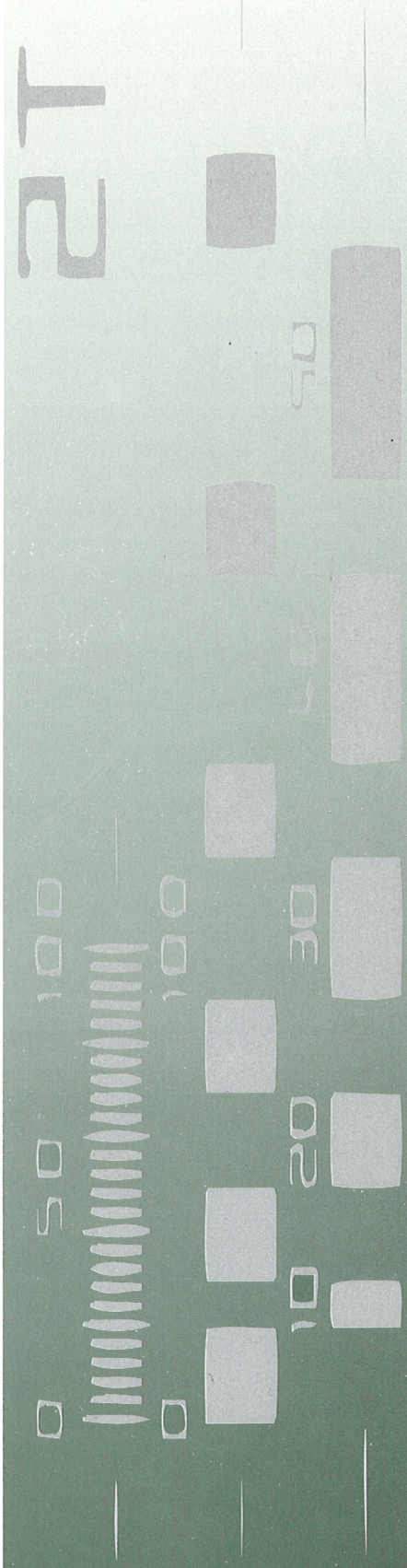
NPL Report CMMT(A)132

REPORT

Code of Practice for Characterising Gas Turbine Blade Coatings

Stuart Saunders, Steve Osgerby,
Jim Banks and Uvais Sheriff

August 1998



NPL
National Physical Laboratory

The National Physical Laboratory is operated on behalf of the DTI by NPL Management Limited, a wholly owned subsidiary of Serco Group plc

NPL Report CMMT(A)132
August 1998

Code of Practice for Characterising Gas Turbine Blade Coatings

by

Stuart Saunders, Steve Osgerby, Jim Banks and Uvais Sheriff

National Physical Laboratory
Teddington, Middlesex, UK, TW11 0LW

ABSTRACT

This Code of Practice describes current best practice for the evaluation of both functional and intrinsic properties of coatings to be used on hot section components of gas turbine engines. The measurement methods described that relate to functional properties are oxidation and hot-salt corrosion resistance, strain tolerance and adhesion of the coating. Strain tolerance encompasses determination of fracture strain, ductile brittle transition temperature and resistance to thermal mechanical fatigue. Description of measurement methods for determination of intrinsic properties is limited to Young's modulus by indentation and residual strain determination by X-ray diffraction measurements.

The methodology described is best current practice, and only in one case (burner rig corrosion testing) has an attempt been made by the international community to validate the test procedures described. This is seen as an important challenge which must be addressed in the short-term. This document, therefore, should be considered very much as a draft for discussion and subsequent development by the gas turbine community.

© Crown copyright 1998
Reproduced by permission of the Controller of HMSO

ISSN 1361-4061

National Physical Laboratory
Teddington, Middlesex, UK, TW11 0LW

Extracts from this report may be reproduced provided the source is acknowledged and the extract is not taken out of context.

Approved on behalf of Managing Director, NPL, by Dr C Lea,
Head, Centre for Materials Measurement and Technology

CONTENTS

1 **INTRODUCTION** 1

2 **SCOPE** 1

3 **GAS TURBINE OPERATING CYCLES** 1

4 **DETERMINATION OF FUNCTIONAL BEHAVIOUR** 2
- **4.1 Oxidation resistance** 3
- **4.2 Hot-salt corrosion resistance** 3
  - *4.2.1 Recommended test method* 4
  - *4.2.2 Assessment of corrosion* 5
  - *4.2.3 Conclusions from VAMAS project and future work* 5
- **4.3 Strain tolerance** 6
  - *4.3.1 Fracture strain* 6
  - *4.3.2 Ductile brittle transition temperature* 9
  - *4.3.3 Thermal mechanical fatigue* 9
- **4.4 Adhesion** 12
  - *4.4.1 Scratch testing* 12
  - *4.4.2 Indentation* 14
  - *4.4.3 Tensile straining* 17
  - *4.4.4 Summary* 18

5 **MEASUREMENT OF INTRINSIC PROPERTIES** 18
- **5.1 Young's Modulus** 18
  - *5.1.1 Description of depth sensing indentation instruments and operating principle* 18
  - *5.1.2 Analysis of load displacement curves* 20
  - *5.1.3 Properties of coated surfaces* 22
- **5.2 Residual stress** 22

6 **CONCLUSIONS** 23

7 **REFERENCES** 23

1 INTRODUCTION

Power generation using gas turbines is becoming an increasingly important part of the energy mix in the UK and worldwide. This is being driven by utilities and large industrial organisations requiring "turn-key" units at competitive prices. Simultaneously there is a drive to increase efficiency as a cost reduction measure. Current and anticipated legislation on the environmental impact of the technology requires attention, and again an effective method of compliance will be the development of more efficient engines burning cleaner fuels. Similar forces are also driving developments in turbines used for aero engines.

Increased efficiency can be achieved in two main ways, by re-design and by an increase in the turbine entry temperature. If the latter stratagem is employed then use of coatings in the high temperature section of the engine will continue to be the main focus of gas turbine development. Thus, it is essential that manufacturers have a well developed system for evaluating and testing coatings used for the advanced engine concepts now at the design stage. This Code of Practice (COP) is an attempt to put such testing on a rational basis.

The COP has been developed during the course of a project funded by DTI as part of its programme of underpinning work on Materials Degradation in Aggressive Environments. This work is set in context with that going on elsewhere and, as will become apparent, further work is required. Some of this work is being carried out in a follow-on project at NPL which is also funded by DTI.

2 SCOPE

The COP concentrates upon corrosion resistant coatings used to protect the blades in the high pressure section of the turbine. Thermal barrier coatings are not considered although some sections on the code of practice may be relevant.

The COP attempts to provide guidance for the measurement of properties of corrosion resistant coatings to be used in the high pressure stages of gas turbine engines. There are many measurement methods that have been devised for determination of these properties, and it would be an unhelpful if all potential methods were described. Some judgement has therefore been made in selecting methods believed to be of general applicability for the systems under discussion. The properties considered relate to their functional performance ie corrosion and oxidation resistance, strain tolerance, [fracture strain, ductile brittle transition temperature (DBTT) resistance to thermomechanical fatigue (TMF)] and adhesion and finally some important intrinsic properties - Young's modulus and residual strain. The intention is to define test procedures that allow engineers to design coating systems for particular operational cycles.

The methodology described is best current practice, and only in one case (burner rig corrosion testing) has an attempt been made by the international community to validate the test procedures described. This is seen as an important challenge which must be addressed in the short-term. This document, therefore, should be considered very much as a draft for discussion and subsequent development by the gas turbine community.

3 GAS TURBINE OPERATING CYCLES

It has been said that no two gas turbines are alike. Even gas turbines operating side-by-side in apparently the same working environment can suffer different extents of corrosion/ degradation. It is, therefore, a difficult task to define "typical" sets of conditions. Nevertheless, an attempt must be made in order to seek to rationalise testing. This is particularly the case for the assessment of corrosion resistance, where changes in fuel and in-take air quality can have a marked effect on degradation.

Three general cases will be considered - aero, marine and land-based use of gas turbines.

For the aero engine cycles can be relatively short (40 minutes) up to about 12 hours with peak operational conditions only experienced at take-off and landing, where maximum blade temperatures can reach 1050 °C - 1100 °C. The bulk of the cycle, however, is at cruise conditions and first row blade temperatures are about 900 °C. The contaminants present in the air are normally present in greater concentrations at or near ground level, and thus the siting of airports is a controlling factor. Alkali metal impurities are generally accepted as being most harmful by forming molten sulphates upon reaction with sulphur present in the fuel during the fuel combustion process. Sea-salt laden air is clearly a hazard and thus frequent flights in and out of coastal airports will be damaging to the engine. Desert air also contains large amounts of sea-salt and similar damage will result. This effect, however, is countered by the fact that the engine is generally at peak power when "dirty" air is encountered so that condensation of sulphate melts may not occur. Service intervals are between 1000 and 5000 h.

Land-based gas turbines operate for longer times at lower temperatures. Typically 900-950 °C for up to 20,000 h between service intervals. The utility market is growing rapidly with the "dash for gas", and in this case fuel purity is generally good, but again the siting of the station will largely control air quality. With natural gas-fired turbines the sulphur content of the combustion gas is so low that attack by condensed sea-salt has been reported [1]. In other cases dirtier fuels are used which may also contain vanadium compounds as well as alkali metals, which further aggravate the problem by the formation of compounds with very low melting point (~500 °C). Thus it can be seen that a great range of behaviour can be expected from the land-based turbine and each turbine installation must be considered separately.

Marine turbines have a more predictable environment, albeit somewhat severe. Here the in-take air is laden with sea-salt and generally a fuel with a defined sulphur level is used, 1 wt% is common. In some cases, there is commercial pressure to use lower quality fuels with higher sulphur contents. This will have the effect of increasing the $p(SO_3)$ and thus help stabilise formation of low melting mixed sulphatic deposits such as $CoSO_4 \cdot Na_2SO_4$ that are known to promote Type II hot corrosion [2]. Type II corrosion occurs in temperature regime 650 - 750 °C and this form of attack is expected to dominate for ship propulsion since much of the operational time of ships will be spent under cruise conditions. Another common application will be as power generators for off-shore oil rigs which will operate at peak temperatures, but fuel quality will be better since natural gas is normally used. The in-take is generally filtered so that the environment at the blade is critically dependent on the effectiveness of these filters.

In all three types of operating environment an important aspect of operation can be erosion as a result of ingested particulate matter or condensed solid phases breaking away from the compressor blades.

4 DETERMINATION OF FUNCTIONAL BEHAVIOUR

Oxidation and hot-salt corrosion resistance need to be determined and an important element of this is cyclic behaviour. It is necessary to simulate closely the thermal cycles experienced in practice since it is known that heating and cooling rates have a major effect on protective oxide integrity [3,4]. In most cases, therefore, burner rig testing is the preferred industrial test method since it is relatively straightforward to achieve the high heating and cooling rates encountered in service. Nevertheless other test methods are used largely because of the high costs of operating a burner rig. Burner rig testing and other test methods are reviewed in the following sections.

Oxidation and corrosion resistance are of little use if the coating cracks or spalls during service, thus strain tolerance and adhesion are essential features in the design of any coating system. The term 'strain tolerance' encompasses a number of specific properties, ie fracture strain, ductile brittle transition temperature (DBTT) resistance to thermomechanical fatigue (TMF), and relate to simple fracture in tension or compression (fracture strain), the temperature dependence of fracture strain (DBTT) and finally in the effect of thermal and mechanical cycles of fracture (TMF). The fracture behaviour of coatings, therefore, is critical to their function and this is also described in this section together with methods to assess adhesion.

4.1 Oxidation resistance

As indicated in Section 3 on Gas Turbine Operating Cycles high temperature oxidation resistance testing is most appropriate for aero applications. For conventional oxidation resistance simple tests are usually carried out in a furnace with the atmosphere chosen to simulate that of the service environment. However a much better simulation is achieved using burner rigs where both the combustion atmosphere is produced and also appropriate thermal cycles can more easily be achieved. Thus oxidation resistance of alloys and coatings used in the gas turbine is generally assessed using burner rigs with combustion of typical aviation fuel. With some of the more complex rigs it is possible to simulate mission cycles [5]; an example is given in Figure 1. More usually these burner rig tests are carried out with simple thermal cycles on approximately hourly time scale. These tests are relatively straightforward and there is general agreement about their suitability to assess accurately cyclic oxidation behaviour.

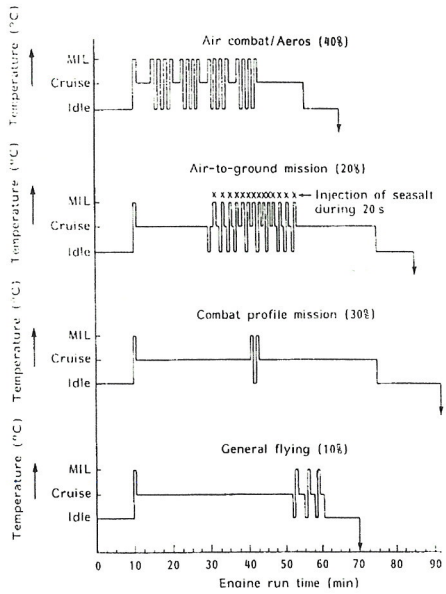


Figure 1 Temperature profiles and occurrence frequency of selected missions for F100 turbine component testing [5]

4.2 Hot-salt corrosion resistance

Hot-salt corrosion is a phenomenon that results when metallic materials are exposed to combustion gases which are contaminated with sulphur and alkali metal salts. Sulphur is usually derived from the use of a fossil fuel and alkali metal salts are often present in the air used in the combustion process. These contaminants combine in the gas phase to form alkali metal sulphates which have relatively low melting points, so that if the component is exposed at a temperature which is below the dew point for condensation of the alkali metal vapours and is above their melting point, molten deposits of the sulphates form on the component. These molten deposits can dissolve the protective alumina or chromia oxide scales that form on the coatings. Two types of attack are common, Type I which corresponds to more generalised attack is usually related to the phenomenon known as basic fluxing where the oxide is dissolved by the molten sulphate deposit to form aluminates or chromates. Type II results in pitting of the alloy and here acid fluxing is the cause with the resultant reaction of the oxide to form Al^{3+} or Cr^{3+} ions [2].

Considerable difficulty has been experienced over the years to develop relevant test methods to assess material behaviour in these conditions. Various tests have been used which include i) a simple furnace tests in which a simulated deposit is placed on the sample and replenished at regular intervals [6]; ii) a Dean test, in which a source of Na_2SO_4 is heated to above about 1100 °C to establish an appropriate vapour pressure and the sample is maintained at a temperature below the dew point to allow condensation of the Na_2SO_4 on the sample [7]; iii) electrochemical tests in which samples are immersed in the molten salt and

the electrochemical parameters monitored [8-10]; and iv) burner rigs in which fuels are burnt to simulate operating conditions closely [11]. In the case of the furnace and the electrochemical tests the gas atmosphere should be controlled to a defined partial pressure of SO_2 [$p(SO_2)$]. There are many variants of burner rigs in use which range from low velocity, atmospheric pressure to high velocity, pressurised systems.

Controversy existed as to which of the simpler tests best simulates service. It was generally acknowledged that high velocity, pressurised burner rigs can accurately reproduce the conditions present in a gas turbine, however, this test procedure is extremely expensive and one which is normally impracticable in most laboratory environments. There have been various attempts to compare the different test methods used, and the earliest of these was a round-robin test initiated by the ASTM in 1970 [12] to study the behaviour of six uncoated alloys. The alloys were exposed at between 884 - 1079 °C for up to 100 h in burner rigs of different design in a set of conditions largely selected by the operator of the equipment. The relative ranking of alloy performance was generally in agreement although there were some notable exceptions, but of more concern was that there was at least an order of magnitude range in the measured corrosion rates.

The ASTM round-robin did not attempt to relate the corrosion product morphology to service experience and was in large measure restricted to burner rig testing. These deficiencies were addressed in a study undertaken within the COST 50 programme on materials for gas turbines [11] which demonstrated that generally good simulation of corrosion product morphology observed on gas turbine blades taken from service was found with samples exposed in burner rigs and some furnace tests. In this work no attempt was made to compare rates of attack in the different test methods, but consideration was given to means of unifying tests methods in order to correlate corrosion rates observed in different designs of burner rig. Earlier work by Hancock [13] had suggested that the contaminant flux rate (CFR) through the gas turbine controlled the overall corrosion rate at a given temperature, but Saunders *et al* [11] proposed that a more important factor was the deposition rate which was related to the contaminant flux rate.

Work was initiated in VAMAS [14] to attempt to build on this prior research to test the thesis that burner rig tests carried out at the same contaminant flux rate would yield similar corrosion rates. It was believed that deposition rates should be the controlling parameter but it was acknowledged that this is difficult to achieve in practice. Thus, in outline, a round-robin test was arranged with both coated and uncoated materials at two temperatures to allow both Type I and Type II hot-salt corrosion mechanisms to be studied for tests lasting 500 h.

An important series of papers was published in a special issue of High Temperature Technology which outlined the VAMAS work and reviewed the topic of hot-salt corrosion testing [15]. As a result of the VAMAS project it has been possible to demonstrate that burner rig can be used in the Type I and Type II corrosion regimes to accurately simulate corrosion found in service. There follows a set of recommendations developed from this work which were designed to simulate corrosion in a marine turbine. These conditions should be modified to take account of the actual operating environment of the turbine. For example at NPL to simulate more closely the condition in an aero turbine the artificial seawater is added only for the first half of each cycle. Detailed results of the VAMAS project can be found in reference 16.

4.2.1 Recommended test method

A summary of proposed test conditions is given below:

Temperature	700 °C and 900 °C
Duration	500 h
Thermal Cycles	once every 10 - 20 h to room temperature
Contaminant Flux Rate (CFR)	4 mg cm^{-2} h^{-1} of sodium added as artificial

	seawater (ASTM D1171-75)
Fuel : Air	1 wt%S at air : fuel ratio of between 30 : 1 and 40 : 1 to achieve 200 - 300 vpm S (as SO_2 and SO_3) in the combustion gas. Otherwise adjust accordingly to achieve desired combustion gas composition.
Test Materials	All materials to be tested in triplicate
Assessment of Deposition	Test conditions to be characterised by monitoring deposition rates using inert specimens and determining the mass change and from chemical analysis (Pt and Al_2O_3 are recommended).

4.2.2 Assessment of corrosion

Samples should be cylindrical in form with no edges (domed tops are recommended) with the initial dimensions of the sample accurately measured and where coatings are used the coating thickness before exposure also must be known.

Three cross-sections should be taken from each sample; one at the mid-point and one each from 10 mm above and below the mid-point. 24 radial measurements should be taken from each cross-section in which the loss of section due to external scale formation, loss of section including grain boundary attack and internal sulphidation should be recorded. The maximum attack at any single point on the circumference of the cross-section is the original radius minus the radius of completely unattacked alloy. In the case of coatings the thickness of any remaining coating should also be measured. These data would enable a full statistical analysis of the tests as recommended by Nicholls and Hancock [17].

4.2.3 Conclusions from VAMAS project and future work

i) This work has demonstrated that attempts to use contaminant flux rate as a controlling parameter in burner rig testing have had some measure of success in allowing rigs of different designs to produce comparable corrosion rates. It was observed however that higher rates were generally observed in the low velocity rigs at 900 °C, and this was attributed to a thicker deposit being present on samples compared to those exposed in the high velocity rigs. While an attempt was made during this work to monitor deposition rates this did not prove particularly successful, but it would seem that quantitative agreement between rigs of different design will only be possible when deposition rates can be controlled.

ii) The scatter in the data produced for coated samples was greater than for the uncoated alloys. It is believed that part of the problem was in assessing the coating microstructures, with different observers making subjective judgments about the extent of attack. Equally, of course there may have been a large variability in the coating quality. It would be extremely valuable for all samples to be measured by a single experimenter to determine whether this scatter was if fact due to measurement errors or coating variability. An omission in this work was that no reference samples were examined by each experimenter, in order that measurement errors could be assessed.

iii) In the case of work carried out at 700 °C, corrosion rate data was more scattered than at 900 °C, and in this case there was no difference between coated and uncoated materials. Unfortunately, only a limited data set was available at this temperature; one from a low velocity rig, one from an ash test and three of the burner rigs which were of shorter durations than specified. The attempt to linearly normalise the results was clearly inadequate because of the effects of incubation periods. It is concluded therefore that there was little gained from this work as no clear results can be established.

iv) An important conclusion which came out of planning this work was that it is essential to increase sulphur levels in fuels when conducting laboratory burner rigs at atmospheric pressure, particularly if

the tests are carried out in the Type II temperature regime. This is necessary to allow for the fact that in a gas turbine the partial pressures of active species such as SO_3 are increased by a factor equivalent to the operating pressure in the turbine [18]. Burner rig testing therefore needs to modified to take account of this important effect.

4.3 Strain tolerance

4.3.1 Fracture strain

A major factor in obtaining reliable measurements of the critical values of failure strain is the method used to detect the first failure event. Acoustic emission (AE) is frequently used thus consideration (in the context of performing the test) must be given to optimising the acoustic signal. However, the substrate response may not allow AE to be used in which case direct observation of cracking must be employed. *In situ* scanning electron microscopy and direct imaging of coating failure is clearly a more time consuming process where, necessarily, the experiment can proceed only very slowly so that the entire sample can be viewed. Test methods are considered in two parts, the first deals with the experimental arrangements for the application of strain and the second with the crack detection system. Since fracture will be related to the presence of any defects in the coating, and these are likely to be randomly distributed, a statistically significant number of tests should be performed (consistent with the accuracy required from the investigation).

4.3.1.1 Application of strain

Two basic methods are considered in this report. Both of these can be carried out at elevated temperature to obtain tensile and compressive data, namely the four-point bend test and conventional tensile and compressive test arrangements modified to allow crack detection. More recently the small punch test has been used to measure the fracture of coatings [19]. This is not considered here, but is the subject of further development in a current NPL project.

Four-point bend tests

Nagl *et al* [20] have described a simple arrangement to obtain fracture strain data using the apparatus depicted in Figure 2. The coated testpiece is first prepared so that a raft of coating is obtained which can be placed between the inner rollers such that it is strained in tension or compression; bottom or top side, respectively. Particular care should be taken to limit damage to the remaining coating raft; in practice it has been found [20] that by using 600 grit SiC paper to remove the excess oxide, damage is confined to within 200 - 500 μm of the edge of the remaining raft. It was also demonstrated that these damaged areas did not act as crack initiators. A standard tensile test machine is used to apply the load to the bend jig.

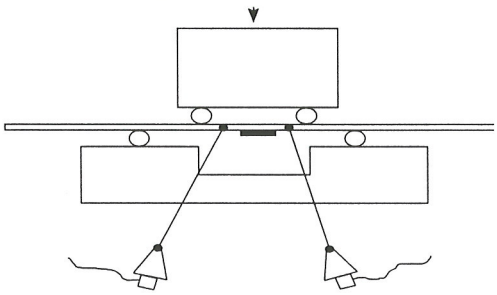


Figure 2 Schematic diagram of four point bend test arrangement

If the tests are carried out at high temperature the testpiece should be prepared as for tests at room temperature and, when assembled in the test jig, raised to the test temperature as quickly as practicable to minimise the formation of an oxide scale on the coating. Experience suggests that with most systems oxide formation is minimal if the tests are carried out within 30 minutes at temperatures below about 1000 °C.

Tests carried out at room temperature use a standard jig made from metallic materials, but for the high temperature tests alumina is employed. Generally the alumina parts are noisier than the metallic jig and

when using AE it is necessary to set higher threshold levels for the high temperature tests. Usually, a small preload is applied so that specimen and jig are in contact and hence, the crosshead movement can be used to calculate the applied strain. However, the preload may cause some deformation and allowance for this deformation is required.

Strain values, ε, from the four-point bend test are given by the following expression:

$$\varepsilon = \frac{3ftd}{u(3s-4u)} \qquad (1)$$

where f is the cross head speed in mm s^{-1}, t is the time in seconds, d is the testpiece thickness, u is the distance in mm between the outer and inner rollers and s is the distance in mm between the outer rollers. The main uncertainty is in the measurement of time to failure as indicated by AE or direct observation. All other parameters can be measured accurately, such that they cause only an overall error of <1%. The error in the measurement of time is absolute, so that at longer times this contribution to the overall error diminished. Typical error analysis yields maximum and mean errors of 15% and 11%, respectively, for a strain of 0.14%, and 10% and 6%, respectively, for a strain of 0.28%.

Checks have been made to establish the validity of equation 1 by use of strain gauges, and up to about 0.3% strain (the elastic region for deformation of most substrate) there was agreement to within 2% of that determined by use of the strain gauge [21]. In the plastic region the calculated values diverged from the measured values as indicated in Figure 3. Thus in the elastic region equation 1 can be used, but in the plastic region deformation has to be checked using strain gauges (this is only possible, for tests up to about 500 °C) or by observing the curvature at the end of the test to see whether it is uniform, i.e. no localized yielding had occurred during the test.

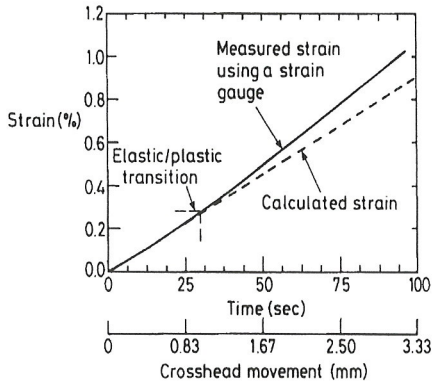


Figure 3 Strain as a function of time or cross-head movement for material tested in tension in a four point bend jig.

Conventional Tensile and Compressive Tests

A test set-up for conventional tests has been described by Schütze [22] and a schematic diagram is shown in Figure 4, and in this case, round tensile testpieces are used. The AE signals are recorded via a waveguide and a stainless steel cone at the transducer, (Figure 4) if tests are performed at elevated temperatures. The waveguide usually consists of a metallic wire and is either clamped or spot welded to the testpiece outside the gauge length. Other waveguide materials can be considered, but the best results were obtained with Pt. Frictional noise may arise from old oxide on the threads of the testpiece grips. Spatial discrimination of noise is possible if two AE transducers are used. This will not always be possible due to the small dimensions of some testpieces and the uncertainties introduced by the waveguide dimensions if two waveguides are used. Therefore, it can be helpful to preload the testpiece close to the elastic limit at room temperature to crack any old scale present in the threads.

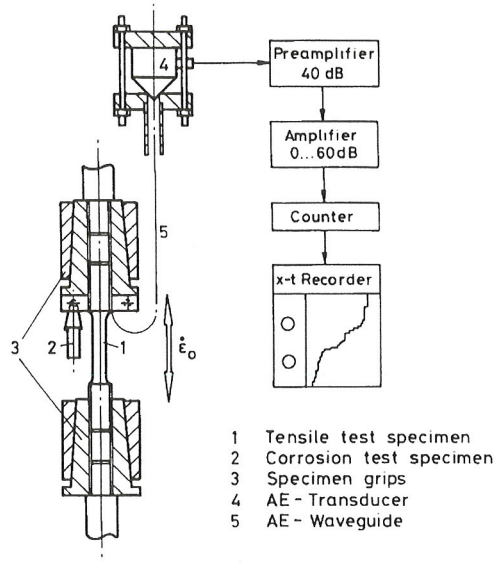


Figure 4 Schematic diagram of experimental arrangement for the measurement of tensile fracture of coatings

Compressive testing is performed analogously [24]. Any lateral bending of the compression rods must be eliminated and the contact surfaces to the testpiece heads should strictly be parallel. Likewise the testpieces themselves must be carefully machined to ensure that opposite faces are parallel. The required axial symmetry of the testpieces can be checked by rolling on a flat surface. Attachment of the waveguide, etc is as for the tensile testpieces.

Strain measurements are made with a transducer that is insulated from the furnace environment. If good temperature stability (~ 1 °C) of the transducer can be maintained, strain can be determined with an accuracy of 2 - 3 μm.

4.3.1.2 Monitoring methods

Acoustic emission

The acoustic signals produced by cracking or spalling events can be detected using a suitable transducer. A large variety of transducers exist, but these can be classified generally as broadband or frequency selective transducers. The latter have the higher sensitivity but have a restricted operational response. Most work to date has been carried out using broadband piezoelectric transducers. If two transducers are used, placed equidistant from the source, events which occur in the region of interest can be selected thereby reducing the background acoustic noise [23]. The transducer should be attached to the testpiece using a viscous couplant (for example Apiezon grease) with a minimum force of 5 N [20].

The system should be adjusted so that background noise is eliminated by setting appropriate threshold values, which are determined by carrying out control experiments, using uncoated testpieces. Failure of the coating is determined by the onset of acoustic activity greater than the threshold level. The precise criteria selected for determination of the critical strain are not generally agreed; some workers take the first signal above the threshold level, while others determine failure to have occurred after the first burst of significant activity. The different approaches could amount to variations in quoted fracture strain values of only about 0.02%. Figure 5 shows a typical set of results as a function of tensile strain (parameter 1)

indicating failure at about 0.5%.

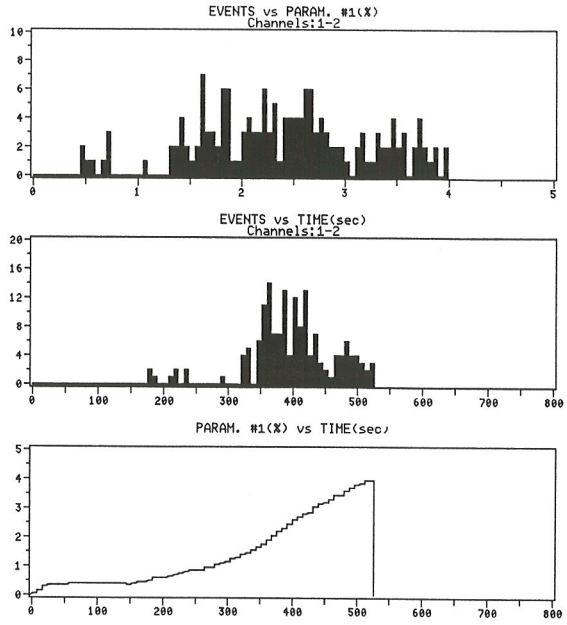


Figure 5 Acoustic emission signals during tensile straining of coated sample

Direct observation

There may be conditions where initial AE experiments indicate the uncoated substrate is itself "noisy" and, although no cracking is observed, it would be impossible to use AE to detect the onset of cracking of the coating. In that case direct observation of the sample using a video system or the use of interrupted tests, with examination of the sample by light or electron microscopy, are the only remaining options. It has been proposed [24] that for samples exposed at high temperatures and examined at room temperature crack detection should be by means of plastic replicas. To ensure the cracks are readily detected a small (0.05%) tensile load is applied before replication of the surface. There is no need to prepare a "raft"of coating if direct observation of cracking is being used.

4.3.2 Ductile brittle transition temperature

Ductile brittle transition temperature (DBTT) measurement is concerned with the determination of the temperature for the effective onset of "ductility". The definition of ductility clearly depends on the application and will need to be expressed as a minimum strain at a given strain rate before cracking occurs. For the case of high temperature blades in gas turbines, 1% strain is considered the maximum likely tensile strain resulting from creep during operation, with about 0.1-0.2% compressive/tensile strain resulting from thermal expansion mismatch between the coating and the substrate depending on whether operating a cooling or heating cycle. DBTT is usually considered with respect to the allowable tensile strain.

Clearly, essentially the same method is used as for the determination of fracture strain except that measurements are focussed on the determination of the temperature at which, say, 1% strain would cause cracking of the coating. The methodology adopted at NPL is to carry out a first test at, say, 700 °C and if cracking occurrs a subsequent test at a higher temperature ,thus progressively defining the DBTT. It has been proposed that where the substrate itself fails before the coating, either deposition on an alternative substrate or stand alone coatings should be investigated. Both approaches have their problems and should be used as a last resort.

4.3.3 Thermal mechanical fatigue

The cyclic operation of a hot-section gas turbine blade causes out-of-phase temperature and strain cycles,

and ultimately coating cracking occurs. Typically gas turbines blades will have a range of different operatingtemperatures. Thus, for example, during heating hot spots will be constrained by the cooler parts of blade and be subject to compression. Frequently the mechanical strain can be out-of-phase with the temperature cycle. If a coating is also present, then depending on the DBTT the accumulated elastic strain during heating can be relieved by creep. On cooling the coating is now placed into tension and cracking occurs if the critical fracture strain is exceeded, see Figure 6.

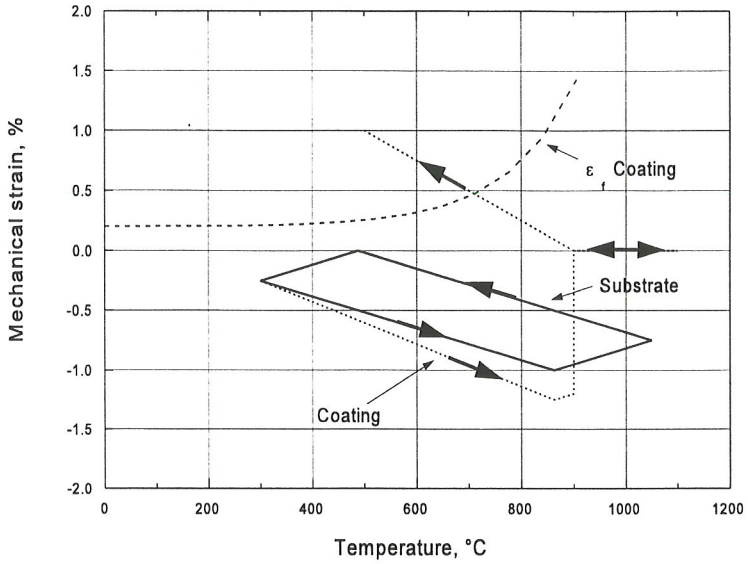


Figure 6 Simulated TMF cycle for substrate and coating

Conventional TMF testing requires both complex testpiece geometry and test equipment (fatigue machines combined with an induction heating system). The objective of the work carried out at NPL was to develop a simplified method based on the principles of the NPL electro-thermal mechanical test (ETMT) [25].

4.3.3.1 Principles of ETMT rig

Essentially a small testpiece is heated resistively and strain cycles applied using a servo-motor. The temperature and strain are monitored and LabView® software is used to control the experimental parameters.

The ETMT rig used for the development of the test had the following specification:

- An environmental chamber (500 x 250 x 120 mm) with comprehensive electrical lead-throughs, water cooling and inert gas supply facilities.

- A computer controlled DC heating power supply (200 A), with testpiece resistance and thermocouple measurement facility. With nickel-base superalloys testpieces typically 2 x 1 mm in cross-section heating rates up to about 10^6 K h^{-1} are possible. Cooling rates are determined by thermal diffusivity of the testpiece and loss of heat to the grips. This can be about 10^5 K h^{-1}. The temperature is measured directly from a thermocouple welded to the centre of the testpiece. The maximum operating temperature is dependent on the melting point of the material under test, input power and testpiece size.

- A mechanical loading assembly (± 1.0 kN maximum), with a drive assembly and capacitance displacement transducers (0.4 µm resolution) arranged in parallel with the long axis of the testpiece. A flexible grip system and load cell (0.2 N resolution), with computer controlled motor for null, mean, ramping or fatigue load capability (in or out-of-phase dc current cycle) or constant displacement tests

for thermal shock experiments. The motor response is set to between 200-1000 N s^{-1} for fatigue experiments.

- Software is used to monitor and control thermoelectro-mechanical tests and temperature cycles by appropriate feedback control.

Heating/cooling rates

Early trials with coated testpieces 2 x 1 mm in cross-section indicated that edge effects dominated the response with clear evidence that coating cracking initiated at the edge of the testpiece. To overcome this effect larger testpieces are needed and a 3 x 2 cross-section was tried. With the larger specimens however the high heating rates achieved with the smaller testpieces could only just be obtained. It is envisaged that even larger test testpieces with a cross-section of 10 mm^2 will be required in future. It is also suggested that testpieces should be circular in cross-section to eliminate the edge effect altogether. This may not always be possible, particularly when dealing with small test testpieces coated by line of sight processes.

Loading and measurement of strain

The larger testpieces required for coated testpieces could not be strained to the required amount with the servo-motors on the standard design (which have a maximum capability of 1 kN). In assessing the performance of the instrument when working at high loads with the motors in parallel with the testpiece, it was determined that significant skewing of the testpiece gripping assembly occurred. Hence the testpiece was also skewed leading to uncertainty in the measurement of strain. The rig was re-designed to allow the motors to be mounted in-line with the testpiece and so overcome the skewing; this is now the standard design for the NPL ETMT rig.

Given the high loads required for this work, there was some concern that strain measured from capacitance transducers not in direct contact with the testpiece may give misleading results. Two options have been investigated which are expected to work. Firstly, it is possible to connect the capacitance transducers directly to the testpieces, or secondly, if the testpieces can be produced with readily identifiable features in the zone of interest, a video strain measuring system can be employed.

A schematic diagram of the re-designed ETMT system for measurement of TMF resistance of coated testpieces is shown in Figure 7. This concept uses hydraulic actuators which have the advantage of being stiffer and also able to apply higher loads. Strain measurement is by capacitance probes directly attached to the testpiece using spring-loaded ceramic contacts. Further development of the rig is now being undertaken at NPL.

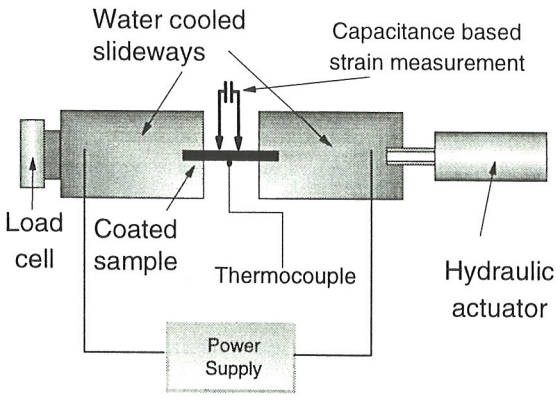


Figure 7 Schematic diagram of the re-designed ETMT-TMF rig

4.4 Adhesion

Three techniques (scratch testing, indentation and flexural straining) with appropriate analyses, have been investigated for measurement of the adhesion of oxide scales and coatings. These methods are appropriate for brittle coatings and, apart from flexure measurements, are conducted at ambient temperature. Previously published analyses have been simplified to enable the techniques to be used more widely. It is concluded that no single technique is applicable to the full range of industrially-important materials and that the investigator must use judgement in the choice of measurement technique and in the interpretation of the results.

There are a large number of tests that can be used to measure adhesion properties and a procedure is required to guide the user to the most suitable test method. The criteria by which tests for scale and coating adhesion must be judged are:-

- generation of a fully-quantifiable output parameter;
- production of a failure mode relevant to service behaviour;
- an output parameter suitable for inclusion in a predictive model;
- suitability for elevated temperature operation.

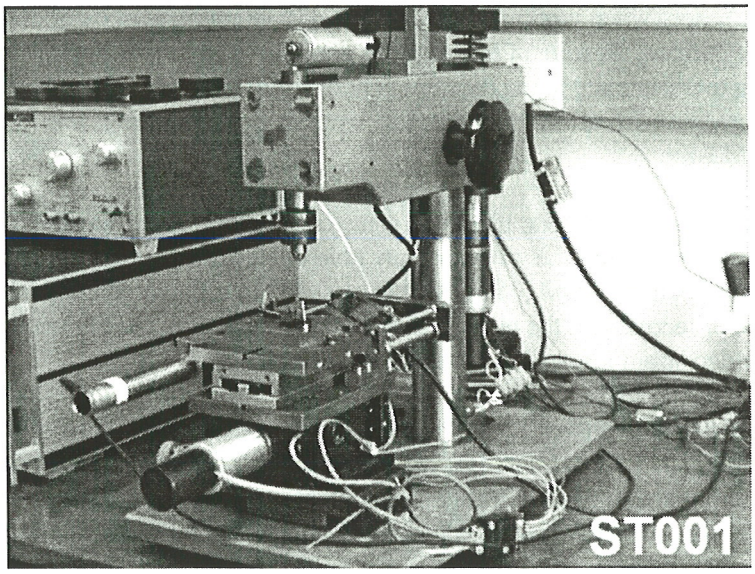


Figure 8 Scratch test facility

4.4.1 Scratch testing

In this form of test a stylus is traversed across the surface of a flat specimen with either constant or increasing load. The experimental set-up for in-plan scratch testing is shown in Figure 8. Specimen preparation is minimal and the only limitation is that the specimen needs to be large enough to clamp without interfering with the movement of the stylus parallel to the plane of the traverse table.

The test parameters that must be monitored are the normal (applied) load and horizontal displacement. It is also desirable to monitor cracking events using acoustic emission (AE) and/or the horizontal (frictional) load. The significant result derived from the scratch test is the critical load for scale failure. This parameter is derived from visual inspection of the scratch track in conjunction with the vertical and horizontal load traces. The derivation is demonstrated in Figure 9.

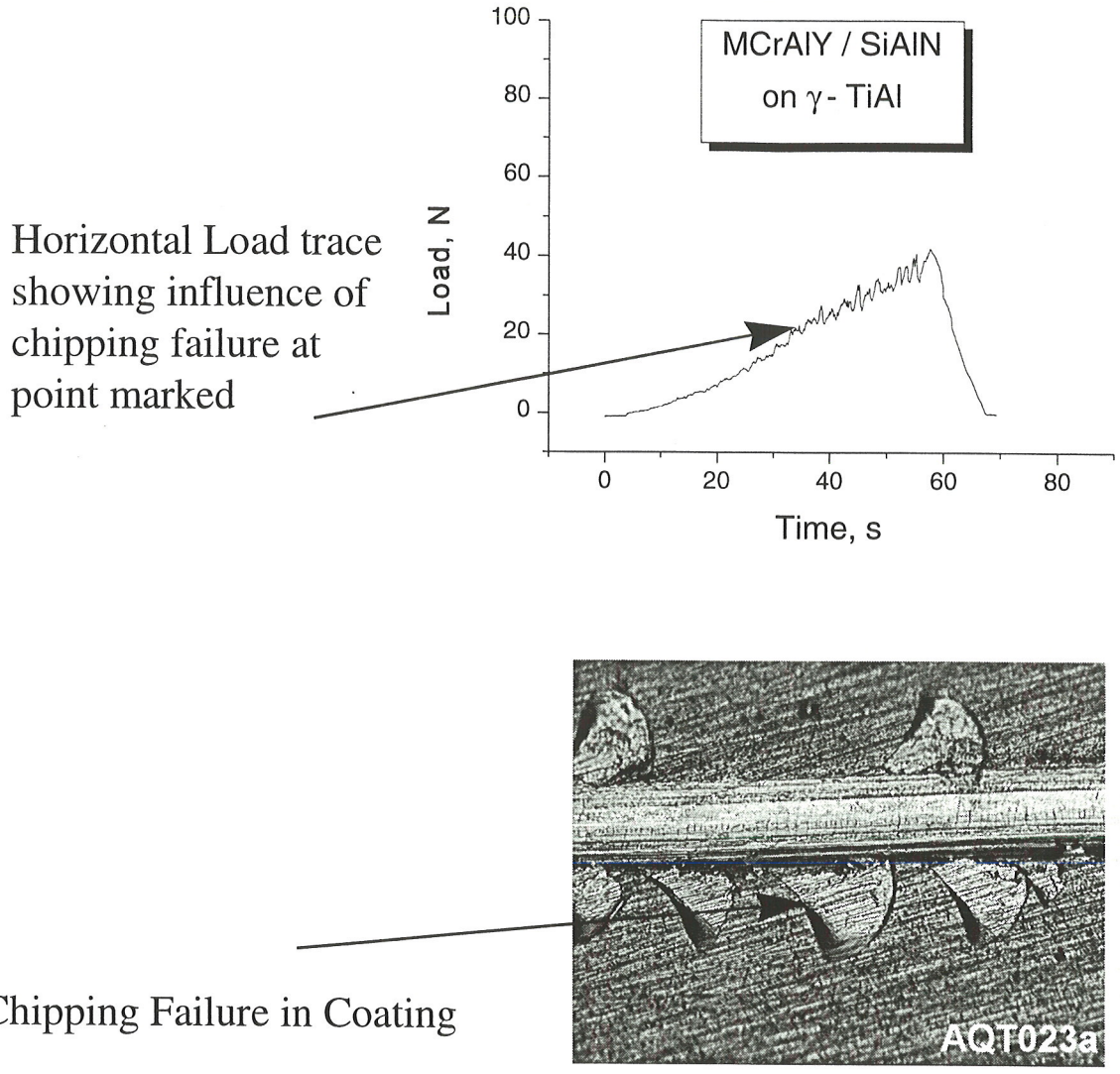


Figure 9 Derivation of critical load during scratch testing for MCrAlY/SiAlN coating on γ TiAl

Failure of the oxide/coating during scratch testing may occur by one of a number of mechanisms [26]. The most important of these, in terms of their relevance to spallation, are buckling and wedge failures. Quantitative interpretation of scratch testing is limited to the latter [27]. The analysis [27], which applies to failure by initial wedge cracking in the surface layer, requires that the critical load for failure is measured as a function of oxide/coating thickness and residual stress.

Ideally a complete matrix of tests should be carried out but, when this is not possible, a multiple linear regression analysis may be used to calculate the output parameters - wedge crack formation stress and interfacial fracture energy. Bull [27] starts from the assumption that the total stress required to detach the surface film, σ_F, is the sum of the residual stress in the film, σ_R, and the stress imposed by the scratch stylus, σ_S. The fracture stress is calculated by a plot of the critical load for spallation as a function of residual stress for a series of surface films of the same thickness. A straight line fit is used and the fracture stress is defined as the intercept ie failure when the imposed stress is zero; the gradient of the line, a, defines the relationship between the critical load in the scratch test and the imposed stress. This can be represented analytically by the expression:-

$$\sigma_F = \sigma_R + aL_c \qquad (2)$$

where

L_c is the critical load measured in the scratch test
aL_c is equivalent to σ_S.

For spallation due to the wedge cracking mechanism, σ_F is the sum of stresses required for wedge cracking, σ_W, and for delamination of the interface, σ_{SP}. Thus

$$\sigma_F = \sigma_W + \sigma_{SP} \quad (3)$$

These terms can be expanded as follows:

$$\sigma_W = \left(\frac{4E_c\gamma}{(1-\nu_c)\lambda} \right)^{½} \qquad \sigma_{SP} = \left(\frac{E_c\gamma_F}{(1-\nu_c)t} \right)^{½}$$

where

E_c and ν_c are the Young's modulus and Poisson's ratio, respectively, of the coating
γ is the fracture energy of the coating
λ is the width of the wedge-spalled region
γ_F is the interfacial fracture energy of the interface
t is the coating thickness

Rearranging and simplifying gives:

$$\sigma_R = A - aL_c + Bt^{\frac{-1}{2}} \quad (4)$$

where A is given by

$$\left(\frac{4E_c\gamma}{(1-\nu_c)\lambda} \right)^{\frac{-1}{2}}$$

and B is given by

$$\left(\frac{E_c\gamma_F}{(1-\nu_c)t} \right)^{\frac{-1}{2}}$$

σ_R, L_c and t can all be measured independently, therefore if at least four tests are carried out the constants a, A and B can be derived using curve fitting procedures (A is normally assumed to be a constant for a given film/substrate system) and γ_F can be calculated from B if E_c and ν_c are also known - E_c can be measured by indentation or vibrational techniques and ν_c is usually attributed the value 0.3.

Scratch testing across the interface of a polished cross-section has been tried with some success for thick thermal barrier coatings and some iron oxides. Here the method relies on the measurement of the critical load to induce cracking at the interface. There is potential for this approach to yield quantitative values of interfacial strength, but to the authors knowledge this has not yet been attempted.

4.4.2 Indentation

Assessment of adhesion from in-plan indentation relies on the measurement of damage around the indent. This type of test is intrinsically simple and can (for room temperature) be carried out on a standard

Rockwell hardness machine. A typical indent is shown in Figure 10. Quantitative analysis follows that derived by Drory and Hutchinson [28] with some modifications to simplify the derivation of scale adhesion parameters. The critical measurements from the indentation are the radii of the indent, a, and of the delaminated area, r.

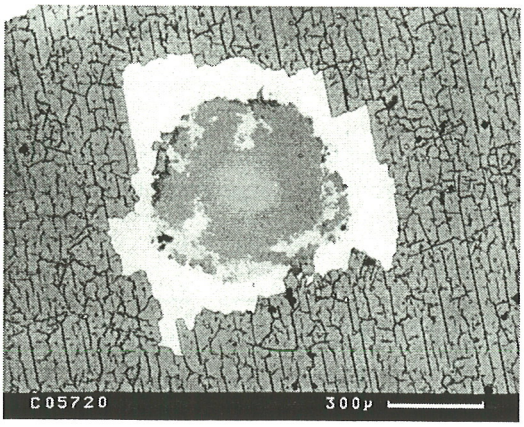


Figure 10 Rockwell indentation of a MCrAlY coating deposited on MarM002

A wide range of other input parameters need to be measured to fulfil the analysis viz thickness Young's modulus, Poisson's ratio and residual stress of the oxide; and Young's Modulus, yield stress and strain hardening exponent of the substrate. These data may or may not be available for the system under investigation, however, they may all be measured independently.

The original analysis by Drory and Hutchinson [28] depends upon the implicit assumption that, at the limit of delamination, the energy needed to cause delamination is in balance with the energy imparted by the indentation process. In order to calculate the latter as a function of radial distance from the indent several properties of the substrate must be known.

It is assumed that the substrate follows a simple deformation law under uniaxial tension of the form:

$$\epsilon = \frac{\sigma}{E_s} + \frac{3}{7}\frac{\sigma_Y}{E_s}\left(\frac{\sigma}{\sigma_Y}\right)^{\frac{1}{N}} \qquad (5)$$

where

- ϵ is true strain
- σ is the applied stress
- E_s is the Young's modulus of the substrate
- σ_Y is the yield stress of the substrate
- N is the strain hardening exponent

The radial surface displacement, u^1, is a function of the normalised distance from the centre of the indent (r/a), σ_Y/E_s, N and Poisson's ratio. In the original analysis [28] this function required a numerical solution, but approximate analytical solutions of the form:-

$$\ln\left(\frac{u^1}{a}\right) = b_0 + b_1\left(\frac{r}{a}\right) + b_2\left(\frac{r}{a}\right)^2 + b_3\left(\frac{r}{a}\right)^3 \qquad (6)$$

were derived for each combination of σ_Y/E_s and N considered. It is obviously desirable to develop an analytical expression that can describe u^1/a as a function of r/a, σ_Y/E_s, and n for the entire range of conditions considered. The following equation provides a reasonable fit:

$$\log\left(\frac{u^I}{a}\right) = 1.917 + 5.706N - 12.97N^2 + 63.99\left(\frac{\sigma_Y}{E_s}\right) - 3203\left(\frac{\sigma_Y}{E_s}\right)^2 - 2.517\log\left(\frac{r}{a}\right) \quad (7)$$

A comparison between this global expression and the original Drory and Nicholson analytical equations is shown in Figure 11. It can be seen that there is good agreement between the expression at all but the lower limits of r/a considered.

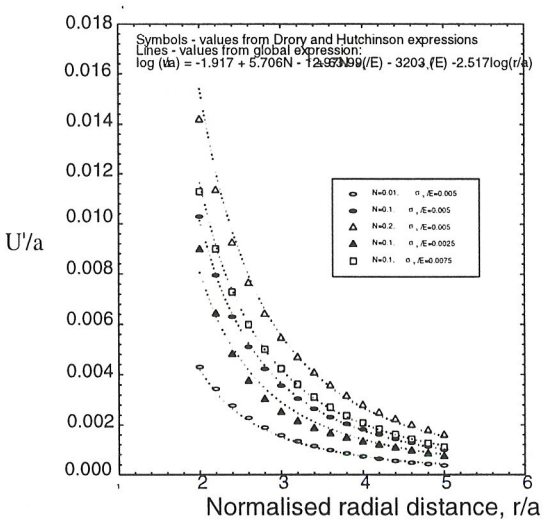


Figure 11 Analytical expression within indentation analysis

The induced radial (ϵ_r^I) and circumferential (ϵ_θ^I) surface strains are then given by:-

$$\epsilon_r^I = \frac{du^I}{dr} \qquad \epsilon_\theta^I = \frac{u^I}{r} \quad (8)$$

These surface strains are then used as in the original analysis to calculate the local radial stress and hence the energy release rate for delamination, G, at any given distance from the indent thus:

$$G = \frac{(1-\nu^2)tE}{2}\left(\frac{\epsilon_0}{1-\nu} + \frac{(\epsilon_r^I + \nu\epsilon_\theta^I)}{1-\nu^2}\right)^2 \quad (9)$$

The interface toughness, Γ_c, is then defined as the value of G at which delamination stops ie at radius r.

The interface toughness is related to the fracture toughness , K_{1c}, of the interface by the expression:

$$\Gamma_c = \frac{K_{1c}^2}{E_{ox}} \quad (10)$$

This method was used to study the effect that different processing conditions had on the interfacial fracture toughness of a MCrAlY coating. In some cases there was no delamination and either radial cracks were observed or there was no damage. Annealing at 1200 °C reduced or eliminated delamination for some types of coating which had values for interface toughness in the range 7 to 15 MN $m^{-3/2}$. Surprisingly, annealing had the opposite effect for coatings of similar composition but with different gas content, and here the interface toughness ranged from 10 - 18 MN $m^{-3/2}$.

4.4.3 Tensile straining

The most convenient method to introduce a uniform tensile strain into a specimen is by flexure in a 4-pt bending rig (see Figure 2). Interfacial shear stress is obtained from the minimum crack spacing after continued bending sufficient to induce spallation of the coating (in contrast to the tests to determine fracture strain). Straining is carried out at a constant crosshead speed, usually ~0.1 mm s^{-1}, although at room temperature the exact speed is not important. Various analyses of the results [29-34] from this type of test are available and have recently been reviewed [35]. The conclusion of this review indicate that the most appropriate model is that of McCartney [33], which is based upon the shear-lag concept of stress distribution. The input parameters required by the McCartney model are:- minimum crack spacing (2L); scale thickness (b); substrate thickness (2a); Young's and shear moduli of scale and substrate (E^s, μ^s, E^c, μ^c); and the tensile and residual strains in the coating (ϵ_c and ϵ_0 respectively). The maximum interfacial shear stress is then given by the expression:-

$$\tau(y) = - \frac{kb\sigma^c \sinh ky}{\cosh kL} \qquad \textbf{(11)}$$

where

$$k^2 = \frac{3\mu^c\mu^s(aE^s+bE^c)}{abE^cE^s(a\mu^c+b\mu^s)} \qquad \sigma_c = \frac{E_c}{\epsilon_c+\epsilon_0}$$

Typical results for some oxide and coating systems are shown in Figure 12.

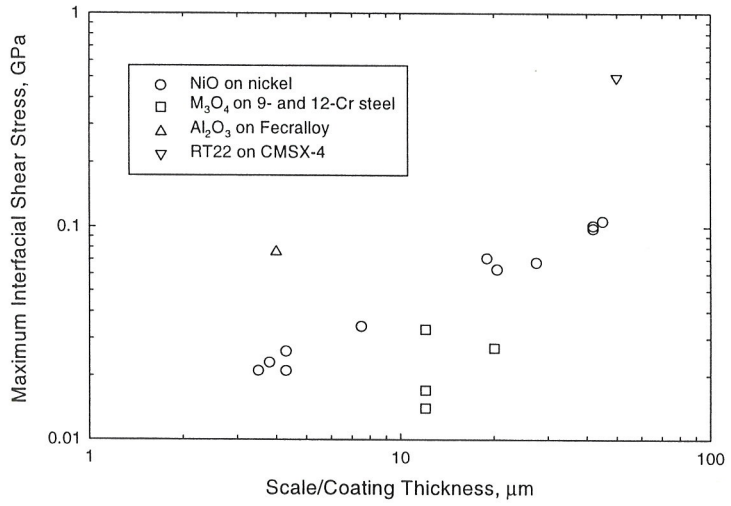


Figure 12 Maximum interfacial shear stress derived from flexural strain tests for different oxide and coating systems

4.4.4 Summary

It is unfortunate that each test generates its own unique parameter for adhesion and that it is difficult, if not impossible to correlate the different parameters. In addition, no single test can be applied to the entire range of coatings. The choice of test method is therefore determined by the material/system to be examined.

Critical load data from the scratch test cannot always be related to an adhesion parameter if the value obtained cannot be related to failure initiated by wedge cracking. The indentation test fails if delamination of the coating cannot be induced. Similarly straining of the coating cannot be quantified if spallation of the coating cannot be induced or if premature failure of the substrate occurs.

Use of the appropriate measurement technique will generate a quantitative value for adhesion, however not all materials can be investigated by the same technique and, at present, it is not possible to correlate the parameters generated by the different techniques. Measurement and interpretation of scale/coating adhesion therefore remains dependent upon the experience of the investigator.

5 MEASUREMENT OF INTRINSIC PROPERTIES

From the previous sections its is clear that two essential properties for modelling are Young's modulus and residual strain. Measurement of these properties is discussed below.

5.1 Young's Modulus

A key input in the design of any component are the Young's moduli of the constituent materials. These data allows calculation of stresses that may be generated in the system. While methods are well established for bulk materials, those applicable to coatings either rely of use of conventional methods and a rule of mixtures to estimate the coating value or require specialist methods that are designed specifically for coatings. One such method is depth sensing indentation (DSI) where elastic properties are derived from the unloading response of an indentation experiment.

5.1.1 Description of depth sensing indentation instruments and operating principle

Determination of hardness and Young's modulus using depth sensing indentation instruments allows direct measurement of these values from indentation experiments where the indentation process is continuously monitored with respect to load and displacement. Indentation experiments may be performed with a variety of differently shaped indenter which are chosen to optimise the plastic and elastic deformation required for a given system. Typically Vickers, Berkovich, conical, spherical and corner cube indenters have been used. Usually an optical microscope is incorporated in the instrument to allow selective positioning of the indents. In some instruments an atomic force microscope is provide to allow imaging of very small indents. This is particularly useful if details of the indentation process are to be investigated. Figure 13 is a schematic representation of a typical instrument.

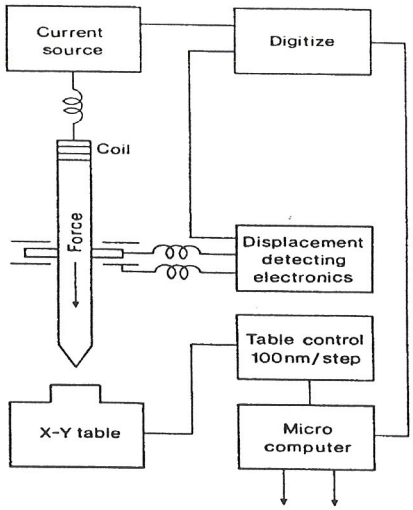


Figure 13 Schematic representation of a typical depth sensing instrument

This experimental method has two major advantages over conventional macro-hardness and micro-hardness test methods. Firstly, subjective estimation of the indent size normally needed for hardness measurement is eliminated from the test, and, secondly, from the same indentation experiment, analysis of the unloading curve allows calculation of Young's modulus.

Displacement is usually measured by a capacitance transducer with a resolution of better than 1 nm, and load is applied and measured by the voltage on a loading coil where resolution of about 100 nN (10 μg) is obtained. Loads and displacements as low as about 50 μN and 10 nm, respectively, can be readily achieved with these instruments, and thus they are extremely powerful for probing the surface of very thin surface layers. Indeed these instruments have been aptly called "mechanical property microprobes" (MPM). It is convenient to classify the instruments as "nano-scale" or "micro-scale" dependent upon the depth resolution obtainable. Typically nano-scale instruments are capable of displacement resolution at the 10 nm level or better while the microscale instruments which generally have a higher load capability and are more reliable at displacements > 0.1μm.

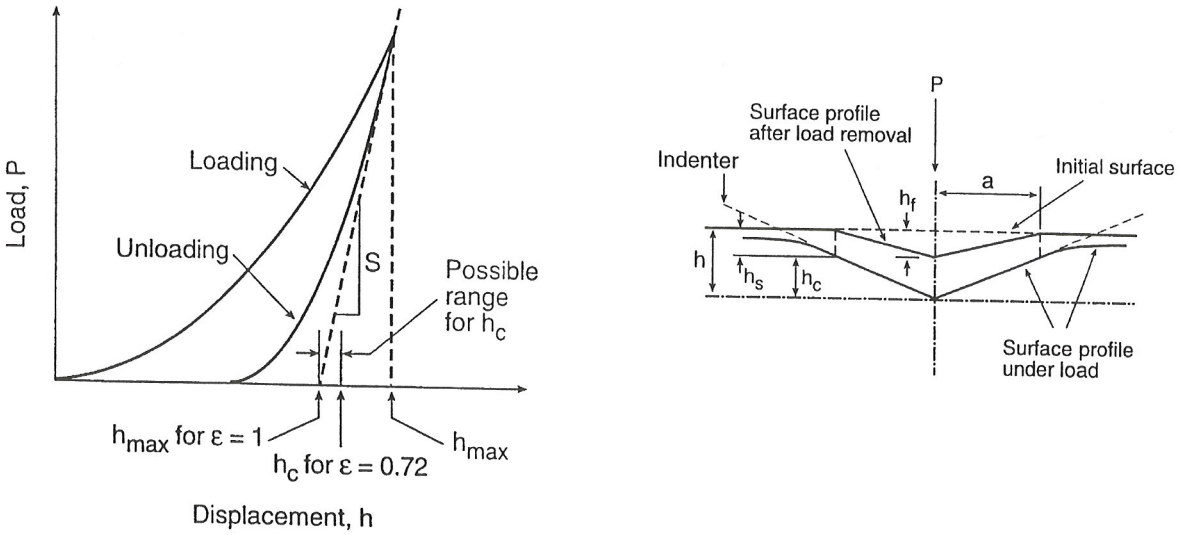


Figure 14(a) Schematic load displacement curve showing the quantities used in the analysis as well as a graphical interpretation of the contact depth, and (b) A schematic representation of a section through an indent showing the various quantities used in the analysis (after Oliver and Pharr, [37])

Figure 14a is a typical load displacement hysteresis curve obtained from an elastic plastic material and Figure 14b is a schematic representation of the indent under load and in the unloaded condition. It is important to note the elastic and plastic contributions to deformation and their derivation on the experimental load displacement curve. Elastic recovery takes place both at the surface and at the base of the indent. The contact depth, h_c, and the final depth, h_f, are related to the "true" and "apparent" hardnesses, respectively, as defined by Sakai [36]. Four parameters are determined: the maximum load, P_{max}; the depth at maximum load, h_{max}; the initial unloading contact stiffness, S; and the contact depth, h_c: the latter two parameters by calculation [37]. It is the definition of h_c that causes most difficulty with this method. Hardness and Young's modulus are then calculated from the following relationships:

$$H = \frac{P_{max}}{A_c} \tag{12}$$

$$E_r = \frac{\sqrt{\pi}}{2}\frac{S}{\sqrt{A_c}} \tag{13}$$

where A_c is the projected contact area at maximum load, S is the stiffness (dP/dh) and E_r is:

$$\frac{1}{E_r} = \frac{(1 - \nu^2)}{E} + \frac{(1 - \nu_i^2)}{E_i} \tag{14}$$

in which E and ν are the Young's modulus and the Poisson's ratio of the sample and E_i and ν_i are the same parameters for the indenter (1141 GPa and 0.07, respectively, are the values for the diamond indenter normally used).

The relationship between the cross-sectional (or projected) area of the indenter and the indentation depth (distance from the indenter tip) is called the area function of the indenter. If this is known, the projected area of contact of the indenter with the sample may be determined from the displacement [38,39]. Assuming all plastic deformation has ceased, the purely elastic contact stiffness is the slope of the unloading curve evaluated at maximum load, P_{max} [40,37]. Various allowances are made for the bowing of the sample in order to determine the correct area of contact. These depend on the geometry of the indenter used. Corrections are also required for the deformation of the whole DSI instrument under load (frame compliance) [37,41]. It is determination of the frame compliance which often requires the use of reference samples and knowledge of the indenter area function. Important corrections required during the analysis are to displacement to account for thermal drift and the indenter tip shape to allow for non-ideal geometry. With suitably calibrated instruments it is possible to achieve repeatability of better than 1% (2 sigma) and 5% accuracy.

Specific test parameters which, if not specified and held constant, may alter the result include: loading rate, unloading rate, maximum load, hold times referenced to the load displacement cycle, indenter geometry and indenter area function, instrument frame stiffness, distance between indents. The effect of changing these parameters will alter dependent upon the material under investigation particularly for materiasls with time dependent properties such as viscoelasticity and creep.

5.1.2 Analysis of load displacement curves

The parameters to be measured are P_{max}, h_{max}, h_c and S. P_{max} and h_{max} can be determined directly from the load displacement curve and S is derived as described above. h_c is required for the determination of the projected contact area which is then given from the indenter area function [$A_c = f(h_c)$]. Hardness and Young's modulus are then computed by use of equations 12, 13 and 14.

Figure 14b shows schematically the different depths monitored during the indentation experiment and these

are related to a typical load unloading curve in Figure 14a. The contact depth, h_c , is derived from the tangent depth, h_t , which is determined by finding the tangent to the unloading curve at maximum load and extrapolating the derived tangent to zero load. The theoretical basis of the method for the determination of contact depth is detailed by Oliver and Pharr [37]. The contact depth is derived from the maximum displacement, h_{max} , via the surface displacement, h_s , as follows:

$$h_c = h_{\max} - h_s \tag{15}$$

and following Sneddon's analysis for a conical indenter [42],

$$h_s = \frac{(\pi - 2)}{\pi} (h_{\max} - h_f) \tag{16}$$

where h_f is the final depth (see Figure 14b). Also for a conical indenter

$$(h_{\max} - h_f) = 2\frac{P_{\max}}{S} \tag{17}$$

thus

$$h_s = \varepsilon \frac{P_{\max}}{S} \tag{18}$$

$$h_c = h_{\max} - \varepsilon(h_{\max} - h_t) \tag{19}$$

where ε is $2/\pi(\pi - 2)$. Thus combining equations 15 and 18, h_c can be derived where ε depends on the indenter geometry and takes the value of 1 for a flat punch, 0.73 [ie $2(\pi - 2)/\pi$] for a conical and 0.75 for a paraboloid indenter.

The major difficulty with this analysis is that no account is taken of the phenomena of pile-up or sink-in. That is material displaced from the indented area is pushed above the initial surface plane and piles-up around the indenter or *vice verse* for sink-in. When pile-up occurs the area in contact with the indenter is increased, thus an adjustment to the contact area should be made. At present this can only be done with the aid of finite element analysis.

Work carried out by Pharr *et al* [43] nicely illustrate this problem. An aluminium alloy sample was stressed by bending and indentation experiments carried out such that regions of the sample in compression and in tension were examined. The simple analysis, as outlined above, showed that the measured hardness varied from about 1.4 - 1.2 GPa on going from the compressive to the tensile stressed (-300 - + 300 MPa) region of the sample. Unfortunately, the values of Young's modulus also varied by about 10%, and since no such dependence would be expected, this clearly raises questions about the procedure used to derive the contact depth. A finite element analysis method was used to calculate the contact area and the solution applied to the calculation of hardness and modulus. When this was done both hardness and modulus were found to be invariant with strain. Whilst this time the expected result was obtained for modulus, the constant hardness was perhaps a surprise in view of the considerable amount of data in the literature, [44] for example) showing increased hardness for compressively stressed samples. Pharr *et al* [43], proposed that pile-up in the conventional measurements also occurred and thus the earlier results were also in error.

5.1.3 Properties of coated surfaces

For indentation in-plan, significant difficulties arise should the load applied be sufficient to cause plastic deformation of the substrate as well as the coating. This is especially the case for thin (less than about 2μm thick) coatings or for measurements made at high loads. The extent of substrate plastic deformation will depend upon a number of factors including the relative difference in hardness and modulus between the coating and the substrate, the coating thickness and the maximum load.

Elastic deformation of the substrate will always occur for all coatings, even though this could be negligibly small for a thick compliant coating on a stiff substrate. There is a practical limit set by the uncertainty of measurement, since elastic stress and strains extend to large distances from the indentation point. The measured Young's modulus therefore will always be the composite modulus of the coating and substrate.

Three approaches can be used to derive the coating hardness and Young's modulus. Firstly, ensure that the maximum load does not exceed a critical value for plastic deformation of the substrate. Empirical guidelines are given in British Standard, BS 5411 Pt 6 [45] for hardness measurement of electroplated coatings on steels, and it is recommended that the indentation depth does not exceed one tenth the thickness of the coating, while for paint films [46] penetration of to up to one third the coating thickness may be allowed.

Secondly, determine experimentally the onset of substrate plastic deformation, and then carry out indentation experiments such that the critical displacement is not exceeded. Different procedures have been published recently which suggest methods that may be used, but none has yet been validated by the international community. These involve a method proposed by Rother, Lunow and Leonhardt [47] in which the differential of the load with respect to displacement is plotted versus displacement, and the point of inflection is taken to be the depth at which plastic deformation of the substrate occurs. Hainsworth, Chandler and Page [48] propose that departure from a linear relationship of load versus the square of displacement is also an indication of the onset of plastic deformation of the substrate. Similar effects were observed by Trindale, Cavalerio and Fernandez [49] when using a log-log plot. Care should be taken when using these approaches for multilayer or graded coatings.

Finally, use an appropriate model that allows calculation of the coating hardness and Young's modulus from the measured composite values. Both analytical and numerical models have been proposed. Analytical models are usually only applicable to elastic deformation. As with the experimental approach, none of these have yet been validated by the international community. For multilayer coatings or coatings with a gradation in properties modelling is clearly much more difficult, and no generally accepted models are available.

5.2 Residual stress

X-ray diffraction (XRD) is commonly used for the measurement of residual strain, and thus if the Young's modulus is known, residual stress can be calculated The principle behind the measurement of residual strain by XRD is that the spacing of interatomic planes in stressed material differs from that in unstressed material. Changes in the interatomic spacing can therefore be related to the *elastic* strain in the material and hence to the stress. The technique involves repeated scanning of a selected peak with the specimen oriented at an increasing angle, φ, to the incident beam (the $\sin^2\varphi$ method). The geometry of the experimental set-up is shown in Figure 15. The shift in interatomic spacing as a function of φ gives the strain according to the expression:-

$$\frac{d_\varphi - d_0}{d_0} = \epsilon_{el}\left(\frac{1+\nu}{1-\nu}\right)\sin^2\varphi \qquad \textbf{(20)}$$

where

d_φ is the measured interatomic spacing at angle φ
d_0 is the measured interatomic spacing at φ=0

ϵ_{el} is the elastic strain in the specimen
ν is the Poisson's ratio of the oxide scale

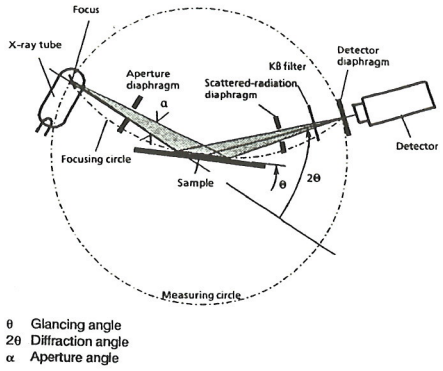


Figure 15 Schematic representation of X-ray diffraction apparatus used in conventional mode

Typically strains in the order of 0.05% can be resolved which gives stresses ~100 MPa [50]. Penetration varies depending upon the radiation source and the diffraction angle; for example, with a Cu Kα source at near normal incidence the maximum penetration would be about 30-40 μm for a compound such as γ-NiAl that would be present in aluminide coatings. .

Care must be exercised to select a peak which is unambiguously identified with the coating under investigation and is sufficiently defined to allow reliable measurement of the interatomic spacings at the different φ. The equipment must also be calibrated by scanning a suitable stress-free (eg powder) sample to identify any peak shift arising from misalignment in the test equipment.

6 CONCLUSIONS

The various test methods that are required to determine service performance of coatings have been described. In only one case (burner rig testing) has the method been evaluated by the international community for the specific case of coatings used in gas turbines, although measurement methods such as XRD, tensile straining, etc. have long been used.

It is recommended that further activity be put in place to validate these and other procedures used by the gas turbine community.

7 REFERENCES

1 F Starr, N Wood and R Robertson, *Journal de Physique, Colloque C9*, **3** (1993) 779

2 J A Goebel, F S Pettit and G W Goward, *Met Trans*, **4** (1973) 261

3 R R Dils and P S Follansbee, *Corrosion*, **33** (1077) 385

4 H E Evans, *International Materials Reviews,* **40** (1995) 1

5 A J A Mom and H J C Herchbach, *Mater.Sci. Eng.*, **87** (1987) 361

6 C H Just, P Huber and R Bauer, *Proc. 13th Int. Congr.on Combustion Engines,* Conseil International des Machines à Combustion (CIMAC), Paris, 1974, Paper GT34

7 A V Dean, "Investigation into the resistance of various nickel and cobalt base alloys to sea salt corrosion at elevated temperatures", *NGTE Rep.,* January 1964 (Royal Aircraft Establishment

Pyestock, Hants.).

8 A J B Cutler and C J Grant, in A B Hart and A J B Cutler (eds.), *Deposition and Corrosion in Gas Turbines*, Applied Science, London. 1973, p.178.

9 D A Shores, *Corrosion,* **12** (1975) 434.

10 A Rahmel, *Werkstoff Korros.*, **28** (1979) 299.

11 S R J Saunders, M K Hossain and J M Ferguson, in R Brunetaud, *et al* (eds.), *High Temperature Alloys for Gas Turbines 1982,* D Reidel Publishing Co., Dordrecht, 1982, p. 177.

12 ASTM Round-Robin Test, 1970 (Hot Corrosion Task Force of Gas Turbine Panel).

13 P Hancock, *Corros. Sci.*, **22** (1982) 51.

14 Proposal for multilateral collaborative research on advanced materials and standards, Summit Working Group on Technology, Growth and Employment, NPL Report, NPL, Teddington, UK, 1983

15 *High Temperature Technology*, **7** (1989) No. 4.

16 S R J Saunders and J R Nicholls, *Materials at High Temperatures*, **13** (1995) 115.

17 J R Nicholls and P Hancock, in R Rapp (ed.), *High Temperature Corrosion,* NACE, Houston, p. 257.

18 K L Luthra, *High Temperature Technology*, **7** (1989) 187.

19 J Kameda and R Ranjan, *Materials Science and Engineering,* **A183** (1994) 121

20 M M Nagl, W T Evans, S R J Saunders and D J Hall, *Mater. Sci. Technol.*, **8** (1992) 1043.

21 M M Nagl, PhD Thesis, University of Glamorgan, UK, *Identification of the Mechanism of Scale Fracture, and its Correlation with Strain Using Acoustic Emission,* 1992.

22 M Schütze, *Oxid. Metals,* **24** (1985) 199.

23 W Christl, A Rahmel and M Schütze , *Mats. Sci. and Eng.* **87** (1987) 289.

24 T E Strangman, "Thermal Fatigue of Oxidation Resistant Coatings for Superalloys", PhD Thesis, University of Connecticut, 1978.

25 B Roebuck and M G Gee, Miniaturised Thermomechanical Tests on Hardmetals and Cermets, *Materials Science and Engineering*, **A209** (1996) 358-365

26 J Meneve, D Havermans, J von Stebut, N M Jennett, J P Banks, S R J Saunders, D Camino, D G Teer, P Andersson and S Varjus, Proc World Tribology Congress, 8-12 Sept 1997, Mechanical Engineering Publications Ltd, London 1997 p 485

27 S Bull ,in 'Advances in Surface Engineering Vol 1 Fundamentals of Coatings', eds P K

Datta and J S Burnell-Gray, Royal Society of Chemistry Special Publication no 206, 1997 pp 274-285.

28 M D Drory and J W Hutchinson, *Proc. R. Soc. Lond.* A **452** (1996) 2319

29 B Y Ting, S Ramalingam, W O Winer, *Journal of Tribology*, **107** (1985) 478.

30 J Armitt, D R Holmes, M I Manning, D B Meadowcroft and E Metcalfe, "The Spalling of Steam-Grown Oxide from Superheater and Reheater Tube Steels", *EPRI report FP 686*, 1978, pp 4-13 to 4-17.

31 D R Wheeler, H Osaki, "Intrinsic Bond Strength of Metal Films on Polymer Substrates - A new Method of Measurement", *American Chemical Society*, ACS Symposium Series 440, 1990, CH 36, p 500.

32 B Burton, *Philosophical Magazine*, **25** (1992) 645.

33 L N McCartney, "Analytical Models of Stress Transfer in Unidirectional Composites and Cross-Ply Laminates, and their Application to the Prediction of Matrix/Transverse Cracking", *Local mechanical Concepts for Composite Material Systems*, 1992, pp 251-282.

34 K Mahmood, *PhD Thesis*, 1988, (Cranfield University).

35 G Damerell, NPL Report CMMT(A)39 'Assessment of Simple Models of the Cracking of Coatings Strained under Tension', September 1996.

36 M Sakai, *Acta metall. mater.*, **41** (1993) 1751

37 W C Oliver and G M Pharr, *J Mater. Res.*, 7 (1992) 1564

38 N M Jennett, G Shafirstein and S R J Saunders, Comparison of Indenter Tip Shape Measurement using a Calibrated AFM and Indentation into Fused Silica. Proc. 9th Int. Symp. Hardness Testing in Theory and Practice. Düsseldorf Nov 1995 VDI Berichte, **1194** pp201-210 Publ. VDI-Verlag GmbH Dusseldorf 1995

39 K Hasche, K Herrmann, F Pohlenz and K Thiele, Micro hardness measurement with the aid of calibrated scanning force microscopes, Proc. XIV IMEKO World Congress, **3**, 240 - 245, 6 June, 1997, Tampere, Finland

40 M F Doerner and W D Nix, *J Mater. Res.* **1** (1986) 601

41 J Meneve, J F Smith, N M Jennett and S R J Saunders, *Applied Surface Science*, **100/101** (1996) 64

42 I N Sneddon, *Int. J. Engng. Sci.*, **3**, (1963) 47

43 G M Pharr, T Y Tsui, A Bolshakov and W C Oliver, *Mat. Res. Soc. Symp. Proc.* **338** (1994), 127-134

44 G Sines and R Carlson, ASTM Bulletin 35 (1952)

45 British Standard: BS 5411 Pt6 *Metallic and Related Coatings, Part 6 Vickers and Knoop Microhardness Tests* Committee ST/37, and ASTM Standard: B578-87 - reapproved 1993 *Microhardness Testing of Electroplated Coatings*

46 ASTM Standard: D 1474 *Indentation Hardness of Organic Coatings*

47 B Rother, T Lunow,and G Leonhardt, *Surface Coatings and Technology,* **71** (1995) 229

48 S V Hainsworth, H W Chandler and T F Page, *J Materials Research*, **11** (1996) 1987

49 A C Trindale, A Cavaleiro and J V Fernandes, *J Testing and Evaluation*, **22** (1994) 365

50 J G Goedjen, J H Stout, Qui Guo and D A Shores, *Mater. Sci. Eng.* **A177** (1994) 115.